Microchimica Acta
https://doi.org/10.1007/s00604-019-3470-1

ORIGINAL PAPER

DNA nanotetrahedron linked dual-aptamer based voltammetric aptasensor for cardiac troponin I using a magnetic metal-organic framework as a label

Zibin Luo[1] · Duanping Sun[1,2] · Yanli Tong[3] · Yongsheng Zhong[4] · Zuanguang Chen[1]

Received: 21 January 2019 / Accepted: 29 April 2019
© Springer-Verlag GmbH Austria, part of Springer Nature 2019

Abstract

An ultrasensitive voltammetric aptasensor was constructed to analyze cardiac troponin I (cTnI). It is based on DNA nanotetrahedron (NTH) linked dual-aptamer (dAPT) and magnetic metal organic frameworks (mMOFs) of type Fe_3O_4@UiO-66. Firstly, the DNA NTH linked dAPT (Tro4 and Tro6) were immobilized on a gold electrode for improving the capture efficiency of cTnI. The novel mMOFs Fe_3O_4@UiO-66 was then decorated by Au@Pt nanoparticles (Au@PtNPs), horseradish peroxidase (HRP), G-quadruplex/hemin (GQH) DNAzyme, and two types of aptamers to form signaling nanoprobes. In the presence of cTnI, an aptamer-protein-nanoprobe sandwich-type structure is formed. Afterward, the nanoprobes including enzyme, GQH DNAzyme and Fe_3O_4@UiO-66/Au@PtNP were utilized to catalyze the oxidation of hydroquinone by hydrogen peroxide for the electrochemical signals amplification, typically at a working potential of −0.1 V (vs. Ag/AgCl). The voltammetric signal increases linearly in the 0.01 to 100 ng·mL^{-1} cTnI concentration range, and the detection limit is 5.7 pg·mL^{-1}.

Keywords Biosensor · Dual aptamer · cTnI · Fe_3O_4@UiO-66 · DNA nanostructure

Introduction

Cardiac troponin I (cTnI), it has been recognized as the "gold standard" for the diagnosis of myocardial injury [1]. Lots of innovative methods including electrochemical immunosensing [2], surface plasmon resonance-based immunosensor [3], electrochemiluminescence immunosensor [4], surface acoustic wave immunosensing [5] and colorimetric immunosensing [6] were employed to determinate trace level of cTnI. As these methods are based on a selective antigen–antibody interaction [7], they suffer from many disadvantages, for example, unstable in high temperature, the production of antibodies is costly, difficult to chemically modify the antibodies for biological detection and need to be operated by a skillful staff. Furthermore, it is difficult to popularize them in the clinical setting because of their limitation of immunogenicity. Hence, aptamer, a small sequence of oligonucleotides screened by systematized exponentially enriched ligand (SELEX), was regarded as alternatives to antibodies for capturing specific targets as it provide many merits to overcome the limitations of antibodies [8]. Compared with antibody, aptamer has many advantages including good stability, easy modification and low cost. Thus, aptamer-based electrochemical biosensors have been established to determinate cancer cells [9], proteins [10] and drug [11] because of its low cost, high stability, low immunogenicity and high detection sensitivity.

But many electrochemical aptasensors are based on single aptamer and its sensitivity is not high enough for clinical application. In order to enhance the capture efficiency

Electronic supplementary material The online version of this article (https://doi.org/10.1007/s00604-019-3470-1) contains supplementary material, which is available to authorized users.

✉ Duanping Sun
sundp@gdpu.edu.cn

✉ Zuanguang Chen
chenzg@mail.sysu.edu.cn

[1] School of Pharmaceutical Sciences, Sun Yat-Sen University, Guangzhou 510006, China

[2] Center for Drug Research and Development, Guangdong Pharmaceutical University, Guangzhou 510006, China

[3] Department of Pharmacy, Guangdong Second Provincial General Hospital, Guangzhou 510317, China

[4] East Campus Lab Center, Sun Yat-Sen University, Guangzhou 510006, China

Published online: 23 May 2019

of cTnI, two kinds of aptamers (Tro4 and Tro6) were introduced for targeting cTnI. The aptamer/target dissociation constants for Tro4 and Tro6 is 270 pM and 317 pM respectively [12]. Nevertheless, single-stranded DNA aptamers immobilized on the electrodes have a tendency to entangle and aggregate with each other, make it very difficult to control its density and orientation and reducing the capture efficiency of cTnI. Thus, for the purpose of solving this challenging problems and further improving the capture efficiency of cTnI [13], DNA nanotetrahedron (NTH), one kind of three-dimensional DNA nanostructures, have been introduced to fabricate this electrochemical aptasensor. Generally speaking, DNA NTH was self-assembled from four single-stranded sequences. There are three vertices of the DNA NTH which can be attached to the gold electrode (AuE) by Au-S interaction and the fourth vertex appended with an extended DNA probe can bind with the target. With the merits of specific orientation, high precision, structural stability, mechanical rigidity and convenient synthesis, DNA NTH have been widely used in the field of biosensor to detect protein [14], small molecules [15] and cells [16]. In brief, a DNA NTH coupled with dual-aptamer (dAPT) was introduced for enhancing cTnI protein capture efficiency.

But only using the DNA NTH, the detection sensitivity is not great enough for determination of trace levels of cTnI in the early stage of acute myocardial infarction (AMI). Thus, a variety of electrochemical signal amplification strategies such as nanomaterials [17], rolling circle amplification (RCA) [18], layer-by-layer (LBL) approaches [19], hybridization chain reaction (HCR) [20] have been explored. Among them, the nanomaterials which can carry one or more enzymes have been explored to be a fascinating strategy for signal amplification and applied for protein detection. Thus, an effective strategy based on loading horseradish peroxidase (HRP) and G-quadruplex/hemin (GQH) DNAzyme onto nanomaterials was put forward to improve the sensors sensitivity through enzymatic electrochemical processes.

A novel class of organic-inorganic hybrid porous materials called metal organic frameworks (MOFs) which was built from cluster nodes or metal ion and organic linkers, have received much attention by many research groups and been widely used in catalysis, separation and gas storage because of its flexible structures, unique inner porosity and unprecedentedly high surface area [21]. Magnetic metal organic frameworks (mMOFs), not only own the same properties as MOFs, but also can be easily purified and separated during the synthesis and application processes by introducing an external magnetic field and have been applied in protein separation, drug delivery and mimetic catalysis [22]. (gold core)@(ultrathin platinum shell) nanoparticles (Au@PtNPs), a sort of bimetallic nanostructure with small size and astonishing catalase-like activity, have been used to establish colorimetric sensor [23]. Fe_3O_4@UiO-66, one kind of Zr-based mMOFs, was selected as nanocarrier for the first time. Then, Au@PtNPs were uniformly modified on nanocarrier Fe_3O_4@UiO-66 via the free amino groups to form Fe_3O_4@UiO-66/Au@PtNP for inducing the oxidation of hydroquinone (HQ) with hydrogen peroxide (H_2O_2) due to strong catalytic activity [24].

An electrochemical aptasensor based on DNA NTH linked dAPT modified AuE for cTnI capturing and the nanoelectrocatalysts for signal amplification has been constructed for ultrasensitive detection of cTnI. The aptasensor is consist of two major parts. DNA NTH linked dAPT was decorated on AuE through Au–S interaction for enhancing the capture efficiency of cTnI. Fe_3O_4@UiO-66/Au@PtNP modified with HRP, GQH DNAzyme and two types of aptamers as multifunctional hybrid nanoprobes can be bind with cTnI by the high-affinity between aptamer and cTnI and catalyzing the oxidation of HQ with H_2O_2.

Experimental

Materials and reagents

2-Aminoterephthalic acid (NH_2-H_2BDC), Zirconium chloride ($ZrCl_4$) were supplied from Macklin Biochemical Co., Ltd. (Shanghai, China, http://www.macklin.cn/). Recombinant myoglobin (MYO), recombinant troponin I (cTnI) and enzyme linked immunosorbent assay (ELISA) kit for troponin I was supplied from Cloud-Clone Co., Ltd. (Wuhan, China, http://www.cloud-clone.cn/). Her2 was supplied from Abcam (Shanghai, China, https://www.abcam.com/). Tris (2-carboxyethyl) phosphine hydrochloride (TCEP) was supplied from Sangon Biotech. Co., Ltd. (Shanghai China, http://www.sangon.com/). Dimethylformamide (DMF), horseradish peroxidase (HRP), 6-Mercapto-1-hexanol (MCH), H_2O_2 (30%, *w*/w), hydroquinone (HQ), Iron (III) chloride hexahydrate ($FeCl_3 \cdot 6H_2O$), poly (acrylic acid) (PAA, M.W~3000), urea, ethylene glycol, hexachloroplatinic acid hexahydrate ($H_2PtCl_6 \cdot 6H_2O$, 99.9%), chloroauric acid tetrahydrate ($HAuCl_4 \cdot 4H_2O$, 99.9%), sodium citrate tribasic dehydrate and L-Ascorbic acid (AA) were purchased from Shanghai Aladin Chemistry Co., Ltd. (Shanghai, China, http://www.aladdin-e.com/). All of oligonucleotides were synthesized and purified by Invitrogen Biotech. Co., Ltd. (Shanghai China, https://www.thermofisher.com/). The sequences were showed in Table S1.

10 mM Phosphate buffered saline (PBS) was used to prepare the nanoprobes and 0.1 M PBS was employed as a working solution. Ultrapure water (18.2 MΩ·cm resistivity, Mille-Q, Millipore) was used for all the experiments. All reagents were of analytical grade and were used without further purification.

Apparatus

Transmission electron microscopy (TEM; JEM-1400, Japan, https://www.jeol.co.jp/) and the field emission scanning electron micrographs (SEM; Geminni500, Germany, https://www.fei.com/home/) were used to characterize the structures and morphologies of the nanomaterials. Fourier transform infra-red (FTIR) spectra were obtained on a Fourier transformation infra-red spectrometer coupled with infra-red microscope (IR, EQUINOX 55, Germany, https://www.bruker.com/cn.html). Powder X-ray diffraction (XRD, Empyrean, Netherlands, https://www.malvernpanalytical.com.cn/) was used to investigate the crystal structure of the nanomaterials. Zetasizer Nano ZS90 (DLS, Nano-ZS90, England, https://www.malvernpanalytical.com.cn/) was used to measure the ζ-potentials of the nanomaterials. The UV − vis absorption spectrophotometer (UV, UV-2600, Japan, https://www.shimadzu.com.cn/) was used to measure the concentration of oligonucleotides and characterized the nanomaterials. Multifunctional microplate reader (ELISA, Flex Station 3, America, http://www.moleculardevices.com.cn/) was applied to read out the results of ELISA.

Electrochemical measurements

All electrochemical measurements were carried out by using a RST5100F electrochemical workstation (Suzhou Risetest Instrument Co., Ltd., Suzhou, China, http://www.cnrst.com/). A conventional three-electrode system containing a bare gold electrode (3 mm in diameter) as the working electrode, an Ag/AgCl reference electrode (the KCl concentration in the reference electrode is saturated solution) and a platinum wire counter electrode (Gaoss Union Technology Co., Ltd. Wuhan, China, http://gaossunion.cn.china.cn/) was applied. Electrochemical impedance spectroscopy (EIS) and cyclic voltammogram (CVs) which were performed in 5 mM $[Fe(CN)_6]^{4-/3-}$ solution containing 0.5 M KCl (frequency range of 0.01 Hz to 100 kHz and an amplitude of a 10 mV) was used to characterize the fabrication of aptasensor. The performance of the aptasensor was investigated by Differential pulse voltammetry (DPV) measurements which were performed in 0.1 M PBS (a saline buffer containing 3 mM H_2O_2 and 2 mM HQ). The working parameters were: 50 ms pulse width, 50 mV pulse amplitude, 0.1 s pulse period and voltage from 0.1 to −0.3 V.

Synthesis of Fe_3O_4 nanoparticles

Fe_3O_4 nanoparticles (Fe_3O_4NPs) were synthesized through a hydrothermal method [25]. In detail, 0.54 g of $FeCl_3 \cdot 6H_2O$ was completely dissolved in 20 mL of ethylene glycol to form a uniform solution under ultrasonic and vigorous stirring. Then, 0.192 g of PAA, 1.5 mL of deionized water, and 1.2 g of urea were added successively and was ultrasonicated for 20 min to make sure that PAA and urea were dissolved completely. Afterward, the mixture was sealed in a Teflon-lined stainless-steel autoclave (25 mL capacity) and heated at 200 °C for 12 h. After the autoclave cooled down to room temperature (RT). The black products were separated by introducing an external magnetic field and washed three times with deionized water and ethanol respectively before dispersing in DMF for next experiment.

Synthesis of Fe_3O_4@UiO-66 composites

Fe_3O_4@UiO-66 composites were synthesized according to a literature method with slight modifications [26]. In detail, 25 mg of Fe_3O_4NPs was dissolved in 10 mL of DMF and ultrasonicated for 1 h to make it disperse in the solution uniformly. Then, the dispersion was added to 8 mL of DMF solution which contained MOF precursors including $ZrCl_4$ (56.25 mg) and NH_2-BDC (43.5 mg). Before holding at 100 °C for 24 h, the resulting mixture was placed in a preheated oven at 80 °C for 12 h. After cooling down to RT, the resulting pale brown solid was magnetic separation and washed three times with deionized water and ethanol respectively.

Synthesis of Au@Pt nanoparticles

Au nanoparticles (AuNPs) were first synthesized via reduction of $HAuCl_4$ by sodium citrate. Briefly, 50 mL of 0.01% (*w*/*v*) $HAuCl_4$ solution was heated to boiling under 140 °C with vigorous stirring. Then, 1 mL of 1% (w/v) trisodium citrate was added into the boiling solution. When the color of the mixture became wine red, left the reaction temperature cooled down from 140 °C to 120 °C. Kept it boiling for another 30 min under stirring and then left it cooled down to RT. The AuNP solution was stored at 4 °C for further use. Au@PtNPs were synthesized by a seed mediated growth method according to a literature with slight modifications [23], 15 mL of AuNP solution, 0.160 mL of 10 mM H_2PtCl_6 solution and 9.040 mL H_2O were mixed together, and the solution was heated to 80 °C under stirring. Following that, 0.800 mL of 10 mM AA solution was added drop-wise slowly into the above solution along with continuous stirring. The mixture was then reacted for another 30 min, and its color turned from red to orange-red, indicating the formation of Au@PtNPs.

Synthesis of Fe_3O_4@UiO-66/Au@PtNP nanoelectrocatalysts

Briefly, 25 mL Au@PtNPs was concentrated to 10 mL and added to 1 mL colloidal suspension of Fe_3O_4@UiO-66 (1.0 mg·mL^{-1}). Subsequently, the mixture reacted at RT overnight under shaking. Au@PtNPs were assembled onto Fe_3O_4@UiO-66 through the free amino groups [24]. Then, the products were separated by a magnet and washed with ultrapure water for three times and kept it in ultrapure water for further use.

Synthesis of hybrid nanoprobes

The synthesized Fe_3O_4@UiO-66/Au@PtNP nanoelectrocatalysts were dispersed in 1 mL PBS solution. Then, 50 μL HRP (1 mg·mL^{-1}), 25 μL capture probe 1 (SH-2G-Tro4, 5 μM) and 25 μL capture probe 2 (SH-2G-Tro6, 5 μM) which were pretreated by 1 mM TCEP for 1 h at RT were added to the solution and reacted at 4 °C for 24 h under stirring. Subsequently, in order to form GQH DNAzyme, 0.1 mg hemin was added to the above solution at 4 °C for 2 h. The product was washed with PBS buffer for twice. The synthesized GQH DNAzyme/dAPT/HRP/Au@PtNP/Fe_3O_4@UiO-66 hybrid nanoprobes were stored in PBS solution at 4 °C for further use.

Preparation of DNA nanotetrahedron

DNA NTH were prepared according to the previous report [13]. Briefly, the DNA NTH were self-assembled from the three thiolated DNA strands of 59 nucleotides (THa, THb, and THc) and one aptamer-containing DNA strand of 101 nucleotides (THd1-Tro4 and THd2-Tro6). Before the assembly of NTH, the monomers (THa, THb, THc, THd1-Tro4 and THd2-Tro6) were pretreated with 10 mM TCEP for 2 h at RT to cleave the disulfide linkage. Then the DNAs were mixed equivalently in TM buffer, heated at 95 °C for 10 min, and rapidly cooled at 4 °C for 20 min. The formation of two kinds of DNA NTHs including DNA NTH-Tro4 and DNA NTH-Tro6 were analyzed using 3% agarose gel electrophoresis in TBE buffer at 100 V for 25 min.

Fabrication of the electrochemical aptasensor

The fabrication process of the electrochemical aptasensor for cTnI detection was illustrated in Scheme 1. Firstly, the AuE was immersed in a piranha solution (H_2SO_4:30% H_2O_2 = 3:1) for 15 min. Then, the AuE was polished by 0.05 μm alumina slurry to a mirror-like surface and cleaned by ultrasonication sequentially in ultrapure water, ethanol and ultrapure water for 3 min. After the electrode were further electrochemically cleaned in 0.5 M H_2SO_4, it was rinsed with ultrapure water and dried with nitrogen for further use. Then, 10 μL of 1.25 μM DNA NTH which was prepared by mixing DNA NTH-Tro4 and DNA NTH-Tro6 in equal proportions was dropped on the surface of pretreated AuE and incubated at 4 °C overnight. For removing the unbound DNA NTH, the electrode was washed with ultrapure water gently. Then, the aptamer/AuE was immersed into 100 μL MCH (1 mM) for 60 min to block the non-specific binding sites. After being rinsed with ultrapure water lightly, the modified electrode

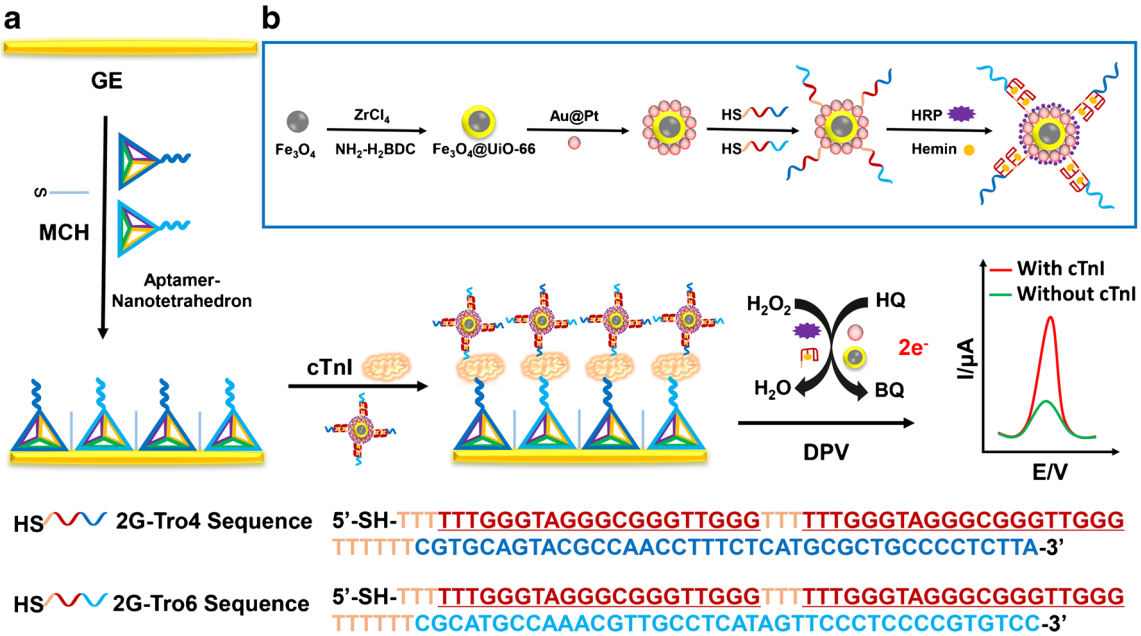

Scheme 1 The synthesis process of GQH DNAzyme/dAPT/HRP/Au@PtNP/Fe_3O_4@UiO-66 nanoprobes and the fabrication processes of the electrochemical aptasensor

was immersed in 100 μL cTnI solution and incubated for 1 h at 37 °C for capturing cTnI. The protein-captured electrode was rinsed with PBS solution gently to remove the dissociative cTnI. Afterward, 10 μL nanoprobes was dropped on it and incubated for 60 min at RT to from sandwich-type aptasensor. Then the electrode was washed with PBS solution lightly for removing nonspecifically bound conjugates. The DPV measurements was performed in degassed 0.1 M PBS containing 2 mM H_2O_2 and 3 mM HQ with potential ranging from 0.1 to −0.3 V and a pulse amplitude of 50 mV.

Results and discussion

Choice of materials and principle of the electrochemical aptasensor

For fabricating an ultrasensitive electrochemical aptasensor, it is vital to select appropriate nanomaterials which can magnify the electrochemical signal and increase the sensitivity of the aptasensor. In this literature, mMOFs Fe_3O_4@UiO-66 was chose as nanocarriers for the following reasons. Firstly, it can be easily separated and purified during the synthesis and application processes by introducing an external magnetic field and recycled if necessary. Furthermore, it has excellent catalase-like activity and can be used as mimetic catalysis [27, 28]. Most of all, unprecedentedly high surface area make it very suitable to load numerous bimetallic nanoparticles. Core-shell bimetallic nanoparticles have showed outstanding catalytic property over the corresponding monometallic nanomaterials [29, 30]. Au@PtNPs have excellent catalase-like activity and can be used to bind with natural HRP and aptamers. Thus, mMOFs Fe_3O_4@UiO-66 was used as a support for the Au@PtNPs. To obtain signal amplification, enzyme was immobilized on the Fe_3O_4@UiO-66/Au@PtNP nanocomposites. To specifically bind with the target cTnI, cTnI aptamer was also loaded on the Au@PtNP/Fe_3O_4@UiO-66 nanocomposites.

The working principle of the fabricated aptasensor is illustrated by Scheme 1. Firstly, the GQH DNAzyme/dAPT/HRP/Au@PtNP/Fe_3O_4@UiO-66 nanoprobes were synthesized (Scheme 1a). Au@PtNPs were assembled onto Fe_3O_4@UiO-66 through the free amino groups, then, the thiolated modified aptamers (SH-2G-Tro4 and SH-2G-Tro6) which integrated with double G-quadruplex sequence were anchor onto Au@PtNPs by the thiol–metal interaction. Then, the natural HRP were decorated onto the Au@PtNPs and the catalytic HRP-mimicking GQH DNAzyme were assembled with the presence of hemin and potassium ion in PBS buffer (Scheme 1b).

Then, the thiolated DNA NTH linked dAPT (Tro4 and Tro6) were immobilized on the AuE surface via Au-S interaction to capture cTnI specifically. After incubating with cTnI and the GQH DNAzyme/dAPT/HRP/Au@PtNP/Fe_3O_4@UiO-66 nanoprobes, an aptamer-protein-nanoprobes super sandwich-type aptasensor was constructed via the high specific recognition and binding affinity between the aptamer and cTnI. In the presence of H_2O_2, the nanoprobes can catalyze the electrochemical reaction of HQ and produced DPV response. As the peak current has a linear relationship with the amount of nanoprobes immobilized on the AuE surface, it indicates the amount of cTnI captured on the AuE surface (Scheme 1b).

Characterization of the nanomaterials

TEM, SEM and UV − vis absorption spectrophotometer was utilized to characterize Fe_3O_4NPs and Au@PtNPs. As we can see from Fig. 1a and d, the Fe_3O_4NPs were spherical with a diameter about 90 nm. As shown in Fig. S1a and Fig. S1b, the Au@PtNPs were spherical and because of the formation of Au@PtNPs, its color turned from red to orange-red. UV − vis absorption spectrophotometer was also used to characterize the formation of Au@PtNPs. As manifested in Fig. S1c, the unshelled AuNPs exhibited a strong localized surface plasmon resonance (LSPR) peak at 520 nm (black line). When the AuNPs were covered with Pt shell, the LSPR peak is blue-shifted to 508 nm (red line). According to the previous studies, the blue-shift maybe stem from the existence of Pt shells on the AuNPs.

The formation of UiO-66 shell on the Fe_3O_4NPs can be initiated by metal ions (Zr^{4+}) chelating with the –OH groups on the Fe_3O_4NPs surface. Afterwards, NH_2-H_2BDC molecules coordinates with the Zr^{4+} ions to form UiO-66. TEM, SEM, Energy dispersive X-ray spectroscopy (EDX) analysis and elemental mapping analysis were utilized to characterize the core–shell structure of the Fe_3O_4@UiO-66 composites. FTIR and XRD were also employed to verify the synthesis of Fe_3O_4@UiO-66 composites is successful. As shown in Fig. 1b, an obvious difference between the core and shell was observe wherein the Fe_3O_4NPs core appeared dark, whereas the UiO-66 shell appeared bright. Compared with the SEM images between Fe_3O_4NPs and Fe_3O_4@UiO-66 composites (Fig. 1d and e), the morphology of Fe_3O_4NPs become irregular and angular after being covered with UiO-66 shell. The EDX spectrum and elemental mapping analysis (Fig. S2) proved that the UiO-66 shell were modified on the surface of the Fe_3O_4NPs. As shown in Fig. S3, after the growth of UiO-66 shell on the surface of Fe_3O_4NPs, its color changes from black to pale brown.

As exhibited in Fig. S4a, the simultaneous existence of the characteristic peaks of Fe_3O_4NPs and UiO-66 in the XRD pattern of Fe_3O_4@UiO-66 indicated the successful formation of a UiO-66 shell on the surface of Fe_3O_4NPs without altering their crystallinity. Fig. S4b shows that the characteristic peaks of UiO-66 at 1564 cm^{-1}, 1430 cm^{-1}, and 1386 cm^{-1} and Fe_3O_4NPs at 1633 cm^{-1} and 565 cm^{-1} in the FT-IR spectrum

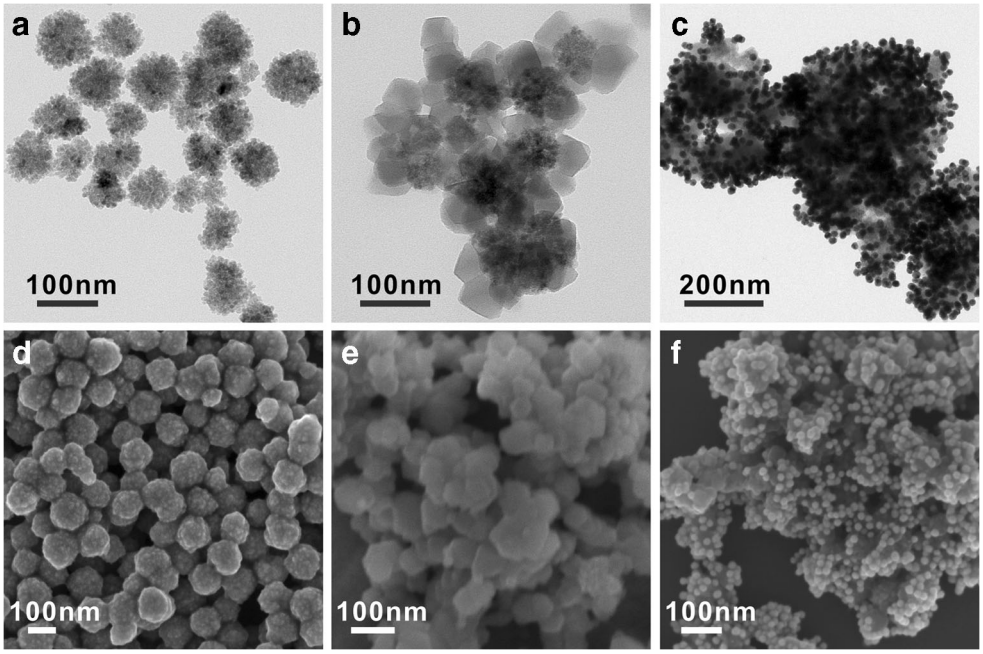

Fig. 1 TEM images of Fe_3O_4 (**a**), Fe_3O_4@UiO-66 (**b**), Fe_3O_4@UiO-66/Au@PtNP (**c**) and SEM images of Fe_3O_4 (**d**), Fe_3O_4@UiO-66 (**e**), Fe3O4@UiO-66/Au@PtNP (**f**)

of Fe_3O_4@UiO-66 indicated the formation of the Fe_3O_4@UiO-66 composites. The peak at 3378 cm^{-1} in the spectrum of Fe_3O_4@UiO-66 belonged to the symmetric stretching absorptions of the primary amine groups in the NH_2–H_2BDC ligands, which further verified the successful growth of the UiO-66 shell on the Fe_3O_4NPs core. All the results demonstrated the UiO-66 shell was successfully grew on the surface of the Fe_3O_4NPs.

TEM, SEM, EDX spectrum, elemental mapping analysis and ζ-potentials analysis were applied to characterize the Fe_3O_4@UiO-66/Au@PtNP nanoelectrocatalysts. As shown in Fig. 1c, f and Fig. S5, Au@PtNPs were uniformly decorated onto Fe_3O_4@UiO-66 through the free amino groups. Furthermore, as exhibited in Fig. S4c, the ζ-potentials of Fe_3O_4@UiO-66 change from positive to negative after Au@PtNPs were assembled on its surface and it also proved that the synthesis of Fe_3O_4@UiO-66/Au@PtNP is successful.

Agarose gel electrophoresis analysis of DNA NTHs

As demonstrated in Fig. 2a, four single stranded oligonucleotides were self-assembled to form DNA NTHs and utilized to enhance the capture efficiency of cTnI. Briefly, one of single stranded oligonucleotide of NTH (THd) was expanded with aptamer, and the other three (THa, THb and THc) modified with thiol groups can be anchor on the electrode.

Agarose gel electrophoretic method was used to verify the formation of NTHs. As exhibited in Fig. 2b, as the molecular weight of the NTH structure (lane 5 and lane 6) are bigger than combinations formed of fewer than four single-stranded oligonucleotides (lane 2, lane 3 and lane 4), they migrated more slowly. Because the DNA hybridization is specific and rapid, the yield of NTHs is high and only one primary clear band can be observed on the agarose gel electrophoretic. The results indicated that the self-assembled of NTHs is successful.

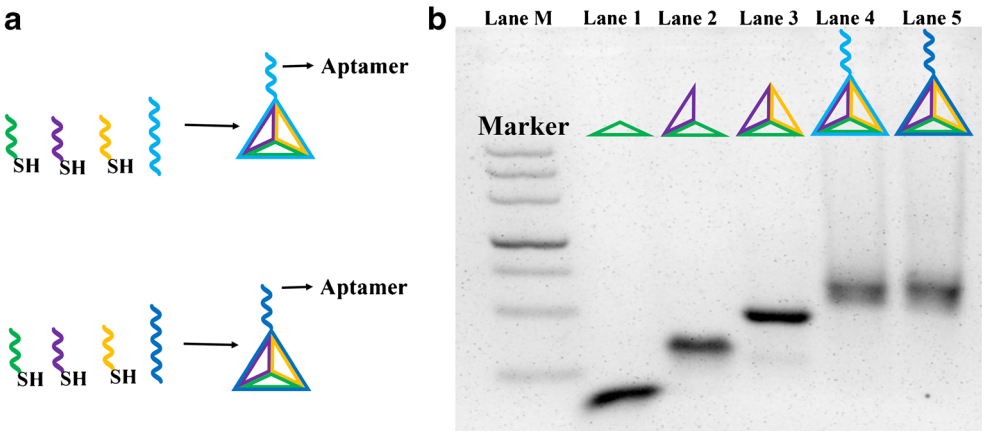

Fig. 2 Self-assembled process of NTHs (**a**), Agarose gel electrophoretic analysis of the gradual formation of NTHs. Lane M: DNA marker; Lane 1: THa; Lane 2: THa + THb; Lane 3: THa + THb + THc; Lane 4: THa + THb + THc + THd1-Tro4; Lane 5: THa + THb + THc + THd2-Tro6 (**b**)

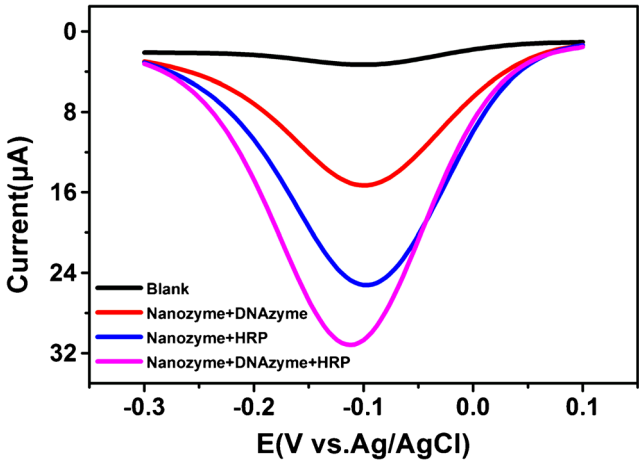

Fig. 3 DPV responses of different signal amplification strategies in the absence (Blank) and in the presence with 50 ng·mL^{-1} cTnI in 2 mL 0.1 M PBS containing 3 mM H_2O_2 and 2 mM HQ by using: (**a**) GQH DNAzyme/dAPT/Au@PtNP/Fe_3O_4@UiO-66 nanoprobes (red line). **b** dAPT/HRP/Au@PtNP/Fe_3O_4@UiO-66 nanoprobes (blue line), **c** GQH DNAzyme/dAPT/HRP/ Au@PtNP/Fe_3O_4@UiO-66 nanoprobes (purple line). Working parameters of DPV: 50 ms pulse width, 50 mV pulse amplitude, 0.1 s pulse period and voltage from 0.1 to −0.3 V

Electrochemical characterization of the aptasensor

According to the Nyquist plots, the charge-transfer resistance (Rct) of the electrode interface is equal to the semicircle diameter of the EIS. So, EIS were applied to confirm the stepwise modification process of the electrode. The results and detailed discussion of EIS are shown in the Electronic Supplementary Material (Fig. S6).

Comparison of different signal amplification strategies

In order to verify the amplification strategies of the aptasensor, a comparative study of the variations of the DPV responses was carried out using different labeled nanoprobes. From Fig. 3, the nanoprobes modified with HRP and Au@PtNPs shows bigger DPV responses variation compared with the nanoprobes decorated with GQH DNAzyme and Au@PtNPs. But when the nanoprobes was labeled with GQH DNAzyme, Au@PtNPs and HRP simultaneously, the electrochemical signal reaches its maximum value. The results indicate that the amplified performance of the nanoprobes may be ascribed to the synergetic catalysis of Fe_3O_4@UiO-66/Au@PtNP, GQH DNAzyme and HRP. Because of its excellent amplified performance, the electrochemical signal of this aptasensor was dramatically amplified.

Optimization of method

In order to maximize the performance of aptasensors, two parameters including the ratio of the two kinds of DNA NTHs and the incubation time of nanoprobes were optimized. Respective data and Figures are given in the Electronic Supporting Material. (Figure S7 and Fig. S8) Experiments show that the aptasensor performs best when the ratio of the DNA NTH is 1:1 (DNA NTH-Tro4: DNA NTH-Tro6) and the incubation time of nanoprobes is 60 min. Therefore, the subsequent experiments were carried out under the best condition.

Analytical performance of the aptasensor in cTnI detection

In order to make an intuitional comparison between ELISA and this electrochemical aptasensor and correct the concentrations of cTnI, ELISA for cTnI detection was carried out simultaneously. As shown in Fig. S9, the absorbance is linear to the concentration of cTnI. The regression equation is A = 0.1892 + 0.0007343 C (pg·mL^{-1}), with a correlation coefficient of $R^2 = 0.9922$. The detection limit is calculated as

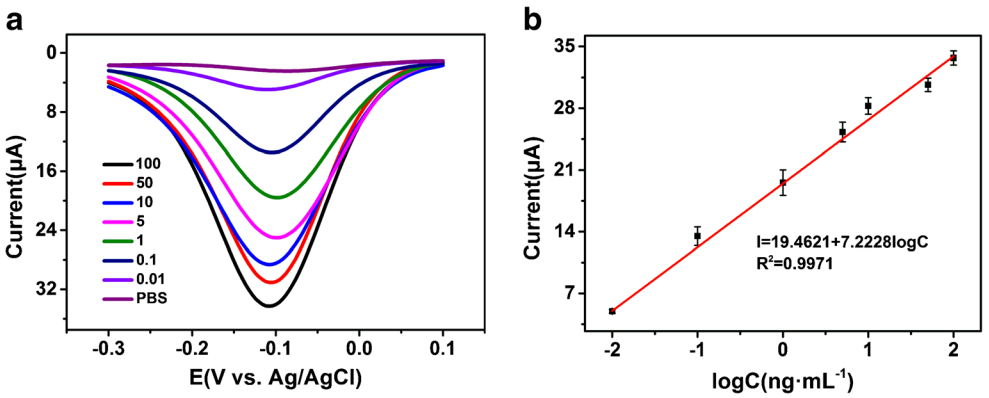

Fig. 4 **a** DPV responses of the aptasensor for the detection of different concentrations (from 0 to 100 ng·mL^{-1}) of cTnI. **b** The calibration plot of the logarithm value of the concentration of cTnI vs DPV response with concentrations range from 0.01 to 100 ng·mL^{-1}, Error bars show the standard deviation of three experiments ($n = 3$). Working parameters of DPV: 50 ms pulse width, 50 mV pulse amplitude, 0.1 s pulse period and voltage from 0.1 to −0.3 V

Table 1 An overview on reported nanomaterial-based electrochemical methods for determination of troponin

Method applied	Materials used	Detection range	Detection limit	Ref
Immunosensor	Silicon nanowire	0.005–5 ng·mL^{-1}	5 pg·mL^{-1}	[2]
Aptasensor	Silica nanoparticles	0.024–240 ng·mL^{-1}	24 pg·mL^{-1}	[12]
Aptasensor	Au nanodumbbells	0.05–500 ng·mL^{-1}	8.0 pg·mL^{-1}	[31]
Aptasensor	N-doped reduced graphene oxide	0.001–100 ng·mL^{-1}	1 pg·mL^{-1}	[32]
Peptide-enabled biosensor	AuNPs	0.0155–1.55 ng·mL^{-1}	3.4 pg·mL^{-1}	[33]
Aptasensor	Fe_3O_4@UiO-66/Au@PtNP nanocomposites	0.01–100 ng·mL^{-1}	5.74 pg·mL^{-1}	This work

15.2 pg·mL^{-1} according to the 3σ method. Afterward, different concentrations of cTnI were detected under optimum experimental conditions for investigating the analytical performance of the electrochemical aptasensor.

As seen in Fig. 4a, when the concentration of cTnI increases from 0.01 to 100 ng·mL^{-1}, the electrochemical signal increases gradually. As shown in Fig. 4b, the DPV peak current is proportional to the logarithm of cTnI concentration in the range from 0.01 to 100 ng·mL^{-1}. The linear regression equation is I = 19.4621 + 7.2228 log C. with a correlation coefficient of R^2 = 0.9971. The detection limit which is calculated according to the 3σ method is 5.74 pg·mL^{-1}. Compared with ELISA carried out for cTnI detection, this aptasensor shows a wider linear range and a lower detection limit. Compared with other electrochemical aptasensor for cTnI detection (Table 1), this aptasensor shows a lower detection limit. However, the application of this aptasensor still exist some challenges such as time-consuming fabrication process and difficulty of clinical application.

Specificity and reproducibility of the aptasensor

The detection result of cTnI in serum sample maybe disturbed by other substances, the selectivity of the aptasensor was evaluated by detecting MYO, Her2, cTnI, the mixture of cTnI and MYO and the blank in the same experiment condition. As shown in Fig. 5, The DPV current response of the no-target protein Her2 (50 ng·mL^{-1}) and MYO (50 ng·mL^{-1}) shows no obvious electrochemical signal change compared with the control group. After incubation with cTnI (50 ng·mL^{-1}) and the mixture of MYO (50 ng·mL^{-1}), the value of DPV peak current increases remarkably indicating that the aptasensor has a high specific affinity for cTnI. These results indicates that the aptasensor had satisfactory selectivity and can be used to detect cTnI in the future. In order to test the reproducibility of the aptasensor, five aptasensors were fabricated and utilized for detecting the same concentration of cTnI (50 ng·mL^{-1}). The DPV responses of each aptasensor shows no significant difference and the relative standard deviation (RSD) is 5.2%, indicating a good reproducibility of the aptasensor.

Performance of the assay in human serum

A further investigation of the applicability of the aptasensor was carried out by detecting the health human serum containing the target protein cTnI which was added according to standard addition method. The results are performed in Electronic supplementary material Table S1. The recovery rate for the cTnI added to the diluted health human serum range from 91.0% to 106.0%. It indicated that the electrochemical aptasensor can be used to detect cTnI in real biological samples potentially.

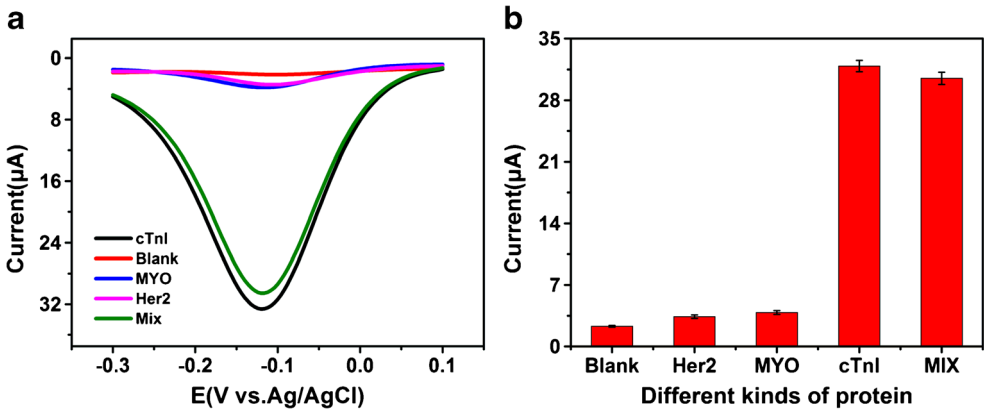

Fig. 5 DPV responses (**a**) and the corresponding histogram (**b**) of the resulting aptasensor toward different analytes. The error bars represent the standard deviations of three parallel determination results (n = 3). Working parameters of DPV: 50 ms pulse width, 50 mV pulse amplitude, 0.1 s pulse period and voltage from 0.1 to −0.3 V

Conclusions

A voltammetric aptasensor based on DNA NTH linked dAPT as capture elements and hybrid nanoprobes for signal amplification was fabricated and successfully applied for ultrasensitive detection of cTnI. Owing to the oriented immobilization of aptamers and high binding affinity between the cTnI and aptamer, the detection sensitivity of cTnI was significantly improved. Benefit from the unprecedentedly large surface area of mMOFs, the hybrid nanoprobes can immobilize more Au@PtNPs, GQH DNAzyme and natural HRP enzyme, amplifying the electrochemical signal dramatically. The aptasensor put up a good performance in cTnI detection with merits of high specificity, good stability, wide linear range and low detection limit. Due to these advantages, electrochemical aptasensors based on DNA NTH linked dAPT and mMOFs provide an important diagnostic technique for cTnI detection. However, the application of this aptasensor still exist some challenges such as time-consuming fabrication process and difficulty of clinical application. In the future, by combining with new technologies such as microfluidic chip, many obstacles will be overcame and this aptasensor will show a great performance in clinical detection.

Acknowledgements We gratefully acknowledge the National Natural Science Foundation of China (No. 21675177), the Natural Science Foundation of Guangdong Province (No. 2018A030310142), the Fundamental Research Funds for the Central Universities (No. 18zxxt69), the Medical Scientific Research Foundation of Guangdong Province (No. A2017033), and the Science and Technology Planning Project of Guangdong Province (No. 2016B030303002).

Compliance with ethical standards The author(s) declare that they have no competing interests.

References

1. Mohammed AA, Januzzi JL (2010) Clinical applications of highly sensitive troponin assays. Cardiol Rev 18:12–19
2. Kim K, Park C, Kwon D, Kim D, Meyyappan M, Jeon S, Lee JS (2016) Silicon nanowire biosensors for detection of cardiac troponin I (cTnI) with high sensitivity. Biosens Bioelectron 77:695–701
3. Kwon YC, Kim MG, Kim EM, Shin YB, Lee SK, Lee SD, Cho MJ, Ro HS (2011) Development of a surface plasmon resonance-based immunosensor for the rapid detection of cardiac troponin I. Biotechnol Lett 33:921–927
4. Li F, Yu YQ, Cui H, Yang D, Bian ZP (2013) Label-free electrochemiluminescence immunosensor for cardiac troponin I using luminol functionalized gold nanoparticles as a sensing platform. Analyst 138:1844–1850
5. Lee J, Lee Y, Park JY, Seo H, Lee T, Lee W, Kim SK, Hahn YK, Jung JY, Kim S, Choi YS, Lee SS (2013) Sensitive and reproducible detection of cardiac troponin I in human plasma using a surface acoustic wave immunosensor. Sensors Actuators B Chem 178:19–25
6. Wu WY, Bian ZP, Wang W, Wang W, Zhu JJ (2010) PDMS gold nanoparticle composite film-based silver enhanced colorimetric detection of cardiac troponin I. Sensors Actuators B Chem 147:298–303
7. Kong T, Su RG, Zhang BB, Zhang Q, Cheng GS (2012) CMOS-compatible, label-free silicon-nanowire biosensors to detect cardiac troponin I for acute myocardial infarction diagnosis. Biosens Bioelectron 34:267–272
8. Medley CD, Smith JE, Tang Z, Wu Y, Bamrungsap S, Tan WH (2008) Gold nanoparticle-based colorimetric assay for the direct detection of cancerous cells. Anal Chem 80:1067–1072
9. Sun DP, Lu J, Chen DB, Jiang YF, Wang ZR, Qin WW, Yu YY, Chen ZG, Zhang YQ (2018) Label-free electrochemical detection of HepG2 tumor cells with a self-assembled DNA nanostructure-based aptasensor. Sensors Actuators B Chem 268:359–367
10. Wang XY, Sun DP, Tong YL, Zhong YS, Chen ZG (2017) A voltammetric aptamer-based thrombin biosensor exploiting signal amplification via synergetic catalysis by DNAzyme and enzyme decorated AuPd nanoparticles on a poly(o-phenylenediamine) support. Microchim Acta 184:1791–1799
11. Zeng RJ, Su LS, Luo ZB, Zhang LJ, Lu MH, Tang DP (2018) Ultrasensitive and label-free electrochemical aptasensor of kanamycin coupling with hybridization chain reaction and strand-displacement amplification. Anal Chim Acta 1038:21–28
12. Jo H, Gu H, Jeon W, Youn H, Her J, Kim SK, Lee J, Shin JH, Ban C (2015) Electrochemical aptasensor of cardiac troponin I for the early diagnosis of acute myocardial infarction. Anal Chem 87: 9869–9875
13. Wang S, Zhang LQ, Wan S, Cansiz S, Cui C, Liu Y, Cai R, Hong CY, Teng IT, Shi ML, Wu Y, Dong YY, Tan WH (2017) Aptasensor with expanded nucleotide using DNA nanotetrahedra for electrochemical detection of cancerous exosomes. ACS Nano 11:3943–3949
14. Wang JP, Leong MC, Leong EZW, Sen Kuan W, Leong DT (2017) Clinically relevant detection of streptococcus pneumoniae with DNA-antibody nanostructures. Anal Chem 89:6900–6906
15. Wen YL, Pei H, Wan Y, Su Y, Huang Q, Song SP, Fan CH (2011) DNA nanostructure-decorated surfaces for enhanced aptamer-target binding and electrochemical cocaine sensors. Anal Chem 83:7418–7423
16. Yang F, Li Q, Wang L, Zhang G-J, Fan C (2018) Framework-nucleic-acid-enabled biosensor development. ACS Sens 3:903–919
17. Sun DP, Lu J, Wang XY, Zhang YQ, Chen ZG (2017) Voltammetric aptamer based detection of HepG2 tumor cells by using an indium tin oxide electrode array and multifunctional nanoprobes. Microchim Acta 184:3487–3496
18. Sun DP, Lu J, Luo ZF, Zhang LY, Liu PQ, Chen ZG (2018) Competitive electrochemical platform for ultrasensitive cytosensing of liver cancer cells by using nanotetrahedra structure with rolling circle amplification. Biosens Bioelectron 120:8–14
19. Ding CF, Zhang W, Wang W, Chen YY, Li XQ (2015) Amplification strategies using electrochemiluminescence biosensors for the detection of DNA, bioactive molecules and cancer biomarkers. Trac-Trends Anal Chem 65:137–150
20. Chen DB, Sun DP, Wang ZR, Qin WW, Chen L, Zhou LD, Zhang YQ (2018) A DNA nanostructured aptasensor for the sensitive electrochemical detection of HepG2 cells based on multibranched hybridization chain reaction amplification strategy. Biosens Bioelectron 117:416–421
21. Wang H, Jian YN, Kong QK, Liu HY, Lan FF, Liang LL, Ge SG, Yu JH (2018) Ultrasensitive electrochemical paper-based biosensor for microRNA via strand displacement reaction and metal-organic frameworks. Sensors Actuators B-Chem 257:561–569
22. Kurmoo M (2009) Magnetic metal-organic frameworks. Chem Soc Rev 38:1353–1379
23. Gao ZQ, Tang DY, Tang DP, Niessner R, Knopp D (2015) Target-induced nanocatalyst deactivation facilitated by core@shell

nanostructures for signal-amplified headspace-colorimetric assay of dissolved hydrogen sulfide. Anal Chem 87:10153–10160
24. Chen HF, Cui YL, Zhang B, Liu BQ, Chen GN, Tang DP (2012) Poly(o-phenylenediamine)-carried nanogold particles as signal tags for sensitive electrochemical immunoassay of prolactin. Anal Chim Acta 728:18–25
25. Xu FJ, Cheng CM, Chen DX, Gu HC (2012) Magnetite nanocrystal clusters with ultra-high sensitivity in magnetic resonance imaging. Chemphyschem 13:336–341
26. Zhao HX, Zou Q, Sun SK, Yu CS, Zhang XJ, Li RJ, Fu YY (2016) Theranostic metal-organic framework core-shell composites for magnetic resonance imaging and drug delivery. Chem Sci 7: 5294–5301
27. Zheng TT, Zhang QF, Feng S, Zhu JJ, Wang Q, Wang H (2014) Robust nonenzymatic hybrid nanoelectrocatalysts for signal amplification toward ultrasensitive electrochemical cytosensing. J Am Chem Soc 136:2288–2291
28. Vermoortele F, Bueken B, Le Bars G, Van de Voorde B, Vandichel M, Houthoofd K, Vimont A, Daturi M, Waroquier M, Van Speybroeck V, Kirschhock C, De Vos DE (2013) Synthesis modulation as a tool to increase the catalytic activity of metal-organic frameworks: the unique case of UiO-66(Zr). J Am Chem Soc 135: 11465–11468
29. Wang H, Zhou CX, Sun XL, Jian YN, Kong QK, Cui K, Ge SG, Yu JH (2018) Polyhedral-AuPd nanoparticles-based dual-mode cytosensor with turn on enable signal for highly sensitive cell evalution on lab-on-paper device. Biosens Bioelectron 117: 651–658
30. Sun XL, Wang H, Jian YN, Lan FF, Zhang LN, Liu HY, Ge SG, Yu JH (2018) Ultrasensitive microfluidic paper-based electrochemical/visual biosensor based on spherical-like cerium dioxide catalyst for miR-21 detection. Biosens Bioelectron 105:218–225
31. Negahdary M, Behjati-Ardakani M, Sattarahmady N, Yadegari H, Heli H (2017) Electrochemical aptasensing of human cardiac troponin I based on an array of gold nanodumbbells-applied to early detection of myocardial infarction. Sensors Actuator B-Chem 252: 62–71
32. Chekin F, Vasilescu A, Jijie R, Singh SK, Kurungot S, Iancu M, Badea G, Boukherroub R, Szunerits S (2018) Sensitive electrochemical detection of cardiac troponin I in serum and saliva by nitrogen-doped porous reduced graphene oxide electrode. Sensors Actuators B Chem 262:180–187
33. Wang B, Jing R, Qi HL, Gao Q, Zhang CX (2016) Label-free electrochemical impedance peptide-based biosensor for the detection of cardiac troponin I incorporating gold nanoparticles modified carbon electrode. J Electroanal Chem 781: 212–217

Publisher's note Springer Nature remains neutral with regard to jurisdictional claims in published maps and institutional affiliations.